I&EC research
Industrial & Engineering Chemistry Research

ARTICLE

pubs.acs.org/IECR

Temperature-Dependent Mechanical Properties and Model of Magnetorheological Elastomers

Wei Zhang,[†] Xinglong Gong,[*,†] Shouhu Xuan,[*,†] and Wanquan Jiang[‡]

[†]CAS Key Laboratory of Mechanical Behavior and Design of Materials, Depasrtment of Modern Mechanics, University of Science and Technology of China, Hefei 230027, China

[‡]Department of Chemistry, University of Science and Technology of China, Hefei 230026, China

ABSTRACT: Magnetorheological elastomers (MREs) are composed of magnetizable particles (iron particles) and a soft rubberlike matrix. Their mechanical properties, including modulus and damping capability, depend on both an external magnetic field and an environmental temperature. To systematically investigate thetemperature-dependent mechanical properties, six different kinds of MREs samples based on a mixed rubber matrices (cis-polybutadiene rubber and natural rubber) and their mass ratios of BR and NR were 100:0, 80:20, 60:40, 40:60, 20:80, and 0:100, were fabricated in this study. The steady-state and dynamic mechanical properties of the samples were measured under different conditions by using a rheometer. The results revealed that storage modulus (G') and loss modulus (G'') of samples, which contained only cis-polybutadiene rubber (BR), decreased linearly with the temperature increment. However, the modulus of sample which contained much natural rubber (NR) showed different characteristic, and the relationships between stress and strain also exhibited different characteristics with different rubber matrix. An improved constitutive equation was developed to model these properties under different magnetic fields and temperatures. The comparison between modeling predicting results with experimental data demonstrated that the model can well-predict the modulus of MRE in different conditions.

1. INTRODUCTION

Magnetorheological (MR) materials represent a kind of intelligent materials whose rheological properties can be controlled rapidly by the application of an external magnetic field. Since the MR effect was discovered by Rabinow in 1948,[1] MR materials have become a large family with MR fluids, MR foams, and MR elastomers (MREs).[2] And MR gels has also been deeply researched in recent years.[3,4] MREs are achieved via the addition of microsized magnetizable particles into the elastomers or rubber-like materials. When such a mixture is exposed to a magnetic field before curing, the field-induced interactions between particles can result in the formation of an anisotropic ordered preconfiguration such as chain-like or more complex three-dimensional structures. After the mixture is cured or cross-linked, these structures are locked into place.[5−9] When the as-prepared MREs are exposed to an applied magnetic field, the field-induced dipole magnetic forces between the particles result in the field dependence of mechanical performance. The change of the modulus is usually termed as MR effect.

MREs are promising for many applications, including adaptive tuned vibration absorbers, stiffness tunable mounts and suspension, and variable impedance surfaces.[10−15] MRE devices often work in some special conditions, such as high pressure and wide temperature range. Thus, the stability or life span of the MRE materials plays an important role in practical MREs applications. In other words, it is crucial to investigate the properties and model MREs under different temperatures or after fatigue and aging. To date, temperature-dependent behaviors and their influence on shear stresses of magnetorheological fluids have once been studied by Zschunke.[16] Davis developed a new model to describe the properties of MREs. The ultimate response of magnetoelastic elastomers containing magnetized Fe particles has been calculated in this work.[17] Dorfmann et al. also have developed constitutive modeling of magneto-sensitive cauchy-elastic solids, and they have summarized the complete system of constitutive equations for an isotropic magneto-sensitive Cauchy-elastic solid within the framework of the electrodynamical and thermomechanical theories.[18] Recently, Li's group has extensively investigated on the theory and applications of MREs. The magnetorheological effect of bimodal particle based MREs and viscoelastic properties of MREs under harmonic loading have been deeply researched in their works.[19,20] Temperature-dependence properties of magnetorheological materials such as MRGs have been researched by Sahin, and in their works MRGs were studied to examine the temperature effect on their yield stress and apparent viscosity.[21] Moreover, the durability of MREs under different temperature has also been investigated.[22] Therefore, studies on the temperature-dependent mechanical properties of the MREs have become a pressing need not only for fundamental interest but also for their practical application. However, there is little work to address this important issue of MR materials.

To experimentally and theoretically investigate the effect of temperature on mechanical properties of MREs, we synthesized a series of mixed rubber matrices-based MREs samples. The mechanical properties of MREs based on different rubber matrix are evaluated by using a rheometer. An improved constitutive

Received: February 25, 2011
Accepted: April 19, 2011
Revised: April 13, 2011
Published: April 19, 2011

dx.doi.org/10.1021/ie200386x | *Ind. Eng. Chem. Res.* 2011, 50, 6704–6712

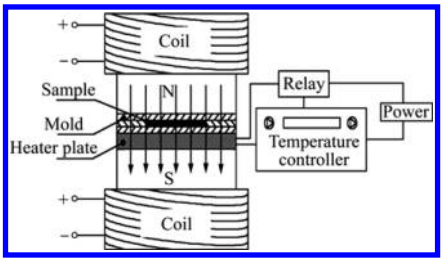

Figure 1. Schematic diagram of prestructure device.

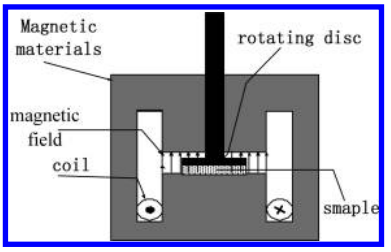

Figure 2. Principle diagram of MR device of rheometer.

equation was developed to model properties in the different magnetic fields and different temperatures. This work would be used in predicting the trend of modulus of MREs under different temperatures and the applied field.

2. EXPERIMENTAL SECTION

2.1. Sample Preparation. The MRE components include two kinds of different rubbers, *cis*-polybutadiene rubber (BR) and natural rubber (NR), carbonyl iron particles CN (BASF Company), and other additives containing carbon black, ZnO, stearin, MDA (4,4′-methylenedianiline), sulfur, cz (N-cyclohexyl-2-benzothiazole sulphenamide), plasticizer and carbon black.[23] Six samples were fabricated and their mass ratios of BR and NR were 100:0, 80:20, 60:40, 40:60, 20:80, and 0:100, respectively. In all samples, the mass fraction of the carbonyl iron particles was 60%. The fabrication procedure of MREs was as follows: the iron particles and other additives were first mixed into the rubber in a double-roll mill. Then, the resulting material is compression-molded into a mold in the self-developed magnet-heat coupled device, which is composed of a magnetic field, a mold, and a controllable heating system (Figure 1). The device consists of two parts: an electromagnetic device and a hot plate. The electromagnetic device is used to generate a magnetic field, which is controlled by an electrical current and the hot plate is used to control the temperature. During the prestructure process, the mixture is exposed to the magnetic field and tightly fixed with a heat plate for vulcanizing. The externally applied magnetic flux density can be changed from 0 to 1 T. The heat plate is conterminal with a temperature controller whose temperature can be set in the range from 50 to 200 °C. In our experiments, the mixture was exposed to a magnetic field of 800 mT at 160 °C for 30 min, after which was cured at 160 °C for 20 min under a pressure of 1.5 atm. After vulcanizing, the fabrication of the MRE samples was completed.

2.2. Testing. A rheometer (Physica MCR 301, Anton Paar) was used in measuring the mechanical properties of MREs at different temperatures. The rheometer and its working principle were shown in Figure 2. Testing temperatures were controlled by a fluid circulator with water, and magnetic field strength was adjusted by manually controlling the current values supplied to the electromagnetic coil. Each sample size is 10 mm in radius and 1 mm in thickness. The sample was set between rotating disk and the base. When the disk rotated, the sample was deformed in a shear mode. This system applies a fixed oscillatory strain amplitude to the sample and measures the amplitude, phase of the output force, from which the shear storage modulus G', loss modulus G'', and damping factor can be calculated. The MRE samples were tested under different temperatures (20, 30, 40, 50, 60, 70, 80, and 90 °C) and different magnetic fields (from 0 to 800 mT), respectively. The shear frequency is a constant 5 Hz and the maximum strain amplitude is 1%. Each sample was tested for three times at the same condition.

3. RESULTS AND DISCUSSIONS

3.1. Mechanical Properties. The mechanical property of each sample has been evaluated by using a rheometer after different kinds of MREs samples were fabricated. Figure 3 shows the mechanical properties (such as storage modulus G' and loss modulus G'') of the samples with different BR/NR ratios measured under different temperature (ranging from 20 to 90 °C). These data indicate that both the storage modulus G' and the loss modulus G'' of the samples, which contain pure *cis*-polybutadiene rubber (BR), show a decreasing trend with increasing of the temperature. Here, Figure 3a) shows that the modulus is linearly dependent on the temperatures. However, other samples which contain natural rubber, show different properties under various temperatures. As shown in Figure 3d−f, the modulus curves show two distinct transitions: they first decrease with temperature rises and then increase when the testing temperature gets higher.

As show in Figure 3f, the transition temperature appears at 50 °C (323 K) is related to the onset of molecular motion in the crystalline phase and appears as a prominent peak at this temperature. For semicrystalline and crystalline polymers, this transition merges with the αc transition.[24] In this case, the transition only appears in the samples which contain NR component, and the sample with higher NR ratio often shows a more obvious transition. Figure 4 shows modulus of samples with different magnetic field at different temperatures. It can be seen from Figure 4 that the change tendencies of the modulus are similar with the increase of temperatures when the samples are tested under different magnetic field. And it also can be seen that modulus of pure NR samples gets to the lower point when the aging temperature is about 50 °C, which is the transition temperature of performance of NR. Moreover, the experimental data also exhibits the same increasing trend with the increasing of the magnetic flux density under different testing temperature (as shown in Figure 4).

Figure 5a−f shows the relationship between stress and strain of MREs under two testing temperatures of 20 and 90 °C, respectively. As shown in Figure 5a, b, it can be seen that it is linear for samples which contain much BR. However, the relationship between stress and strain is nonlinear if matrix is pure NR (Figure 5e, f). It can also be seen from this figure that nonlinear relationship is more obvious when the temperature gets higher. The adhesion between particle and BR matrix is better than the one between the particle and NR matrix, thus the elastic properties of samples based on BR is better because the adhesion between particle and BR matrix are more stable. The viscoelasticity of the sample which contain more NR is more obviously than others' because the adhesion between particle and NR can be easily destroyed with increasing of the strain amplitude. As shown in Figure 6b, loss factor of MREs based on

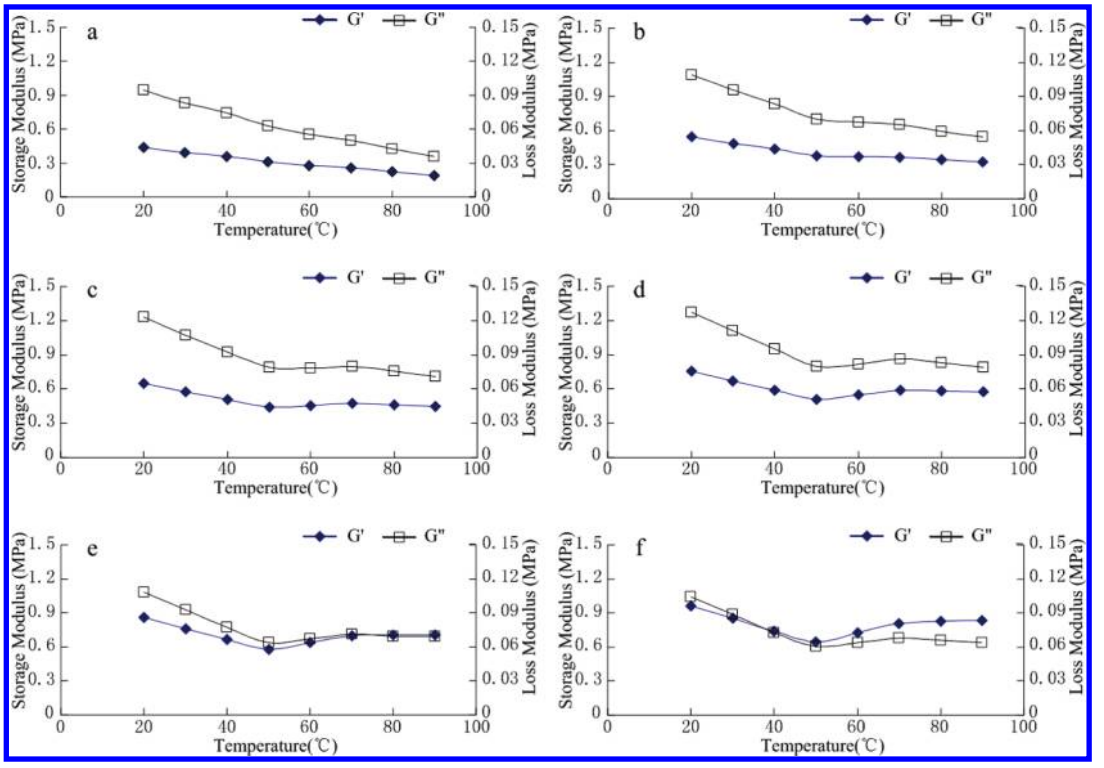

Figure 3. Temperature-dependent modulus of samples with different ratios of BR/NR (800 mT): (a) 100:0, (b) 80:20, (c) 60:40, (d) 40:60, (e) 20:80, and (f) 0:100.

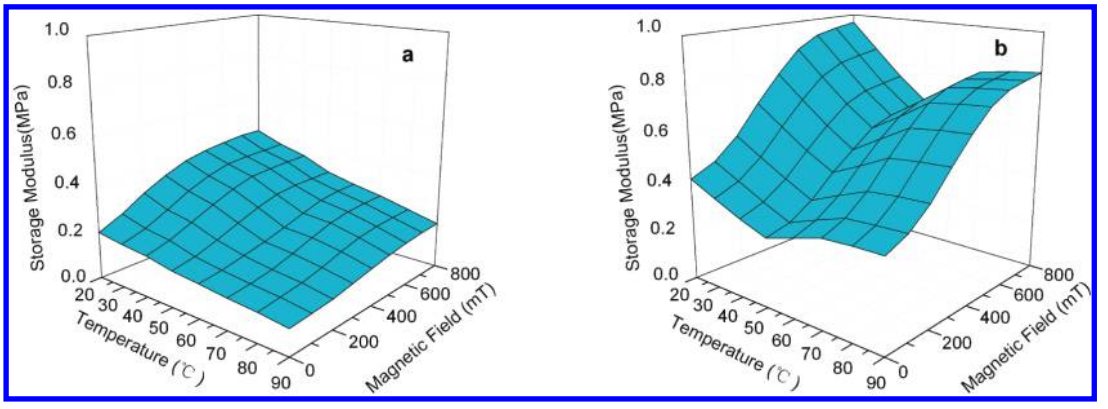

Figure 4. Temperature-dependent modulus of samples with different magnetic field (a) BR/NR 100:0, (b) BR/NR 0:100.

NR increases obviously when the adhesion is destroyed, which can enhance nonlinearity of samples. Conversely, samples which contain more BR component have better linear elastic because the damping increases slowly, as shown in Figure 6a.

To study the influence of temperature and strain amplitude, the MRE samples were tested at a fixed frequency of 5 Hz and with magnetic field range from 0 to 800mT. The test strain amplitude was from 0 to 1%. Figure 6 shows the trend of loss factor with increasing of the strain at different temperature. The loss factors of the MREs samples based on different BR/NR ratios were measured at a driving frequency of 5 Hz under various temperatures with the magnetic fields at 800 mT, and the dynamic strain amplitude ranges from 0 to 1%. It can be seen from this figure (Figure 6) that the loss factor of all samples exhibits the increasing trend with increasing of the dynamic strain amplitude. However, each sample has the particular properties. The relationship between loss factor of sample based on pure BR and dynamic strain amplitude is linear at different temperatures, as shown in Figure 6a. Meanwhile, the loss factor of MREs, which contain only NR, increases with increasing of the dynamic strain amplitude. First, the loss factor increases nonlinearly when the strain amplitude is from 0 to 0.4%, and then the damping factor increases linearly when the strain amplitude gets higher, which is noticeable in Figure 6b. Because the adhesion between particle and NR can be easily destroyed, the loss factor of MREs based on pure NR exhibits significant increase when the strain amplitude is small. However, the adhesion between particle and rubber matrix gets to the stable state with increasing of the strain amplitude. Thus, the loss factor increases slowly when the strain amplitude is big.

dx.doi.org/10.1021/ie200386x |*Ind. Eng. Chem. Res.* 2011, 50, 6704–6712

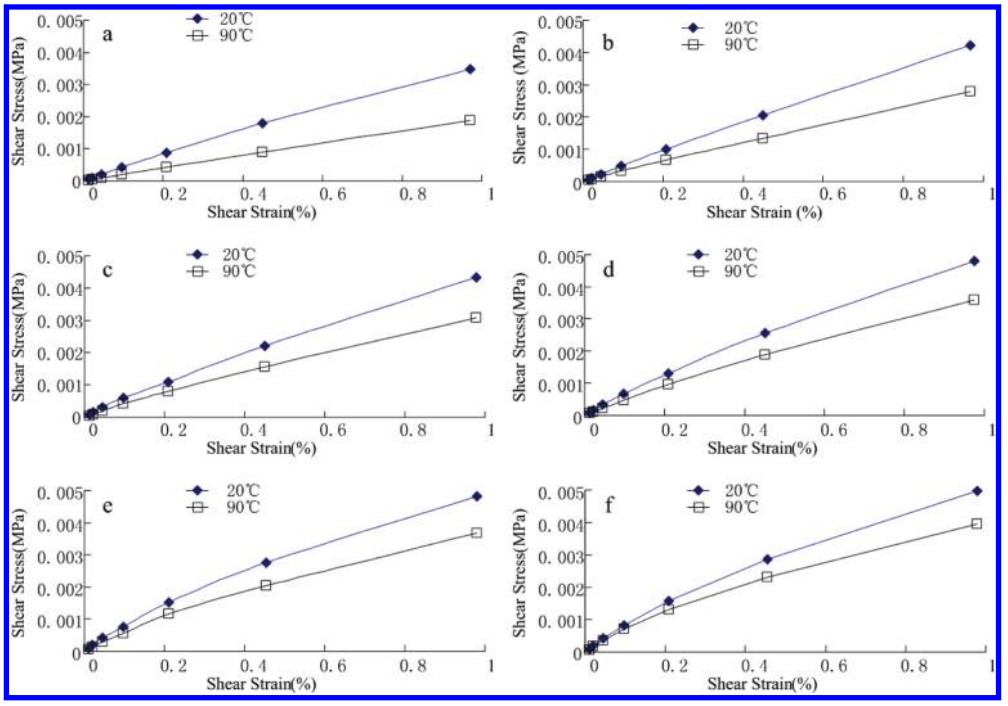

Figure 5. Relationship between stress and strain of samples with different ratios of BR/NR at 800 mT: (a) 100:0, (b) 80:20, (c) 60:40, (d) 40:60, (e) 20:80, and (f) 0:100.

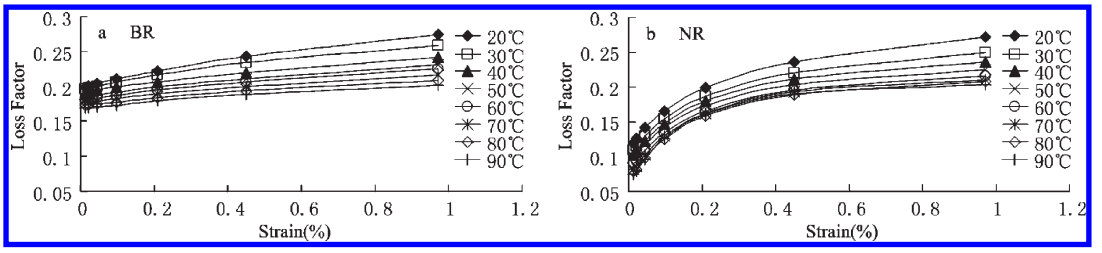

Figure 6. Change curves of loss factor with strain amplitude of MREs at 800mT (a) BR/NR 100:0, (b) BR/NR 0:100.

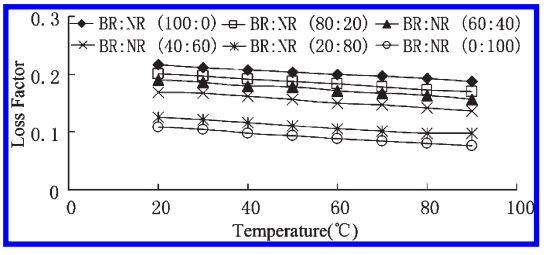

Figure 7. Change curves of loss factor under different temperatures of MREs at 800 mT.

From Figure 7, it can be seen that the damping of all samples are inversely proportional to the temperature. MRE is kind of complex materials with iron particles dispersed in rubber matrix. There are mainly two kinds of damping source for MRE. One is from the rubber matrix, and the other is from the friction between iron particles and rubber matrix.[26] It is because that rubber matrix becomes soft when temperature rises, and then the friction between iron particles and rubber matrix becomes weak. As a result, the damping capability decreases with increasing of the temperature.

In addition, the loss factor of the MREs based on pure NR is lower than that of MREs based on other different ratios of BR/NR (Figure 6). It has been proven that the damping ratio of NR is lower than most rubbers (such as BR and CIIR[25]), which agrees well with our results. Figure 8 shows that with the increment of magnetic field, the loss factor of the MREs samples follow an increasing trend. However, as soon as a maximum value (at about B = 300 mT) was reached, the loss factor changes, following a decreasing trend, consistent with results of previous research.[23]

3.2. Constitutive Model. The microscopic observations of MREs samples (BR/NR 0:100) are shown in Figure 9, and all the six samples with different proportion of BR to NR have the similar the chain like structures. It can be observed that the iron particles are assembled to form chainlike structures and the aligned parallel chains are of different length and width, which indicates the as-prepared product show an anisotropic characteristic. According to our previous report, a Gaussian distribution model was invited to examine the field-induced shear modulus of the anisotropic MR elastomers.[27]

For ER and MR fluids, body-centered tetragonal (BCT) structure was proven to be the most stable field-induced structures in both of the theoretical[28] and experimental[29] studies. A similar structure also has been observed in MREs through a microstructural study.[30] Thus, the as-proposed model is based on

dx.doi.org/10.1021/ie200386x |*Ind. Eng. Chem. Res.* 2011, 50, 6704–6712

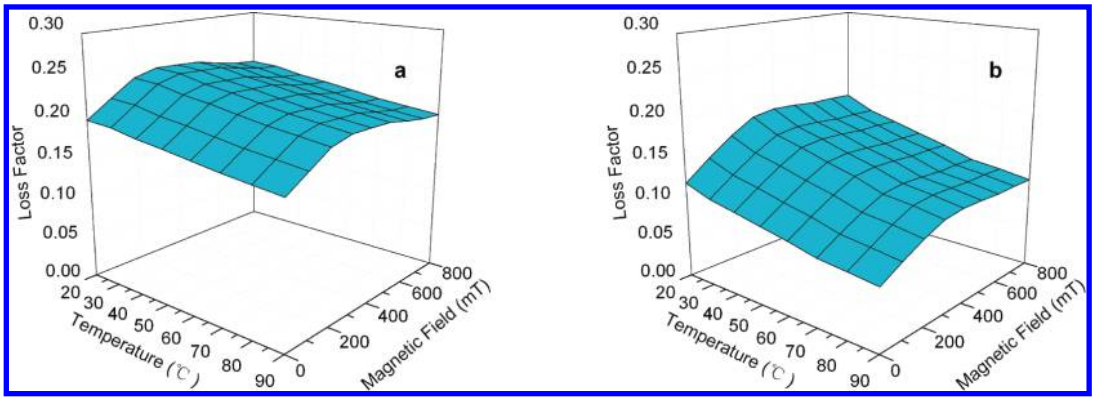

Figure 8. Temperature-dependent damping factor of samples with different magnetic field (a) BR/NR 100:0, (b) BR/NR 0:100.

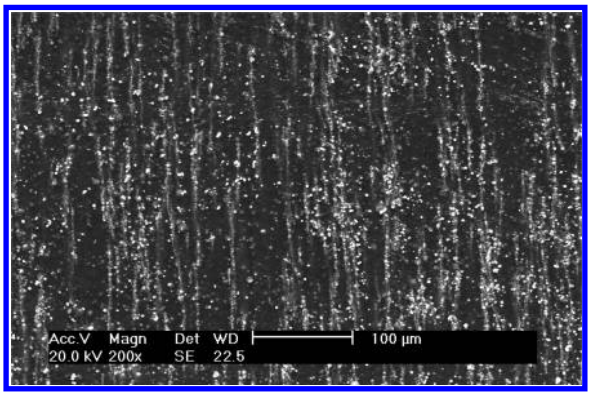

Figure 9. Microscopic observations of MREs samples by SEM (BR/NR 0:100).

the assumption that all the iron particles (2.5 μm) were assembled to a large number of BCT structures, which have the same direction and width but different length (as shown in Figure 10). To further simplify the calculations, it is assumed that all the chains are neat and straight. In addition, we also assume that the column length l' obeys the Gaussian distribution. Thus the numbers of the particles l ($l = l'/2R+1 \geq 1$), along with each column, also obeys the Gaussian distribution where the mean and the variance are represented by L and σ^2 respectively. Due to the symmetry of the Gaussian distribution, the length l is assigned less than $2L$, i.e., $l \leq 2L$. Thus the value of l is distributed on the range of $[1, 2L]$. When the width of the column is b', the number of the particles in the width border is denoted by b where $b = b'/\sqrt{6R+1}$.

In this work, an improved constitutive equation was developed to model the mechanical property of the MRE under different magnetic fields and temperatures, which can be used to predict the modulus and relationship between stress and strain.

Shear stress τ of MREs can be obtained as follows

$$\tau = -\frac{\partial W}{\partial \gamma} \tag{1}$$

γ is shear strain and W is the magnetic energy density. According to research of Bossis,[31] W can be rewritten as

$$W = \frac{1}{2}HB = \frac{1}{2}H\mu_0\mu_{x\text{eff}}H = \frac{1}{2}\mu_0\mu_{x\text{eff}}H^2$$
$$= \frac{1}{2}\mu_0(1+\chi_{x\text{eff}})H^2 \tag{2}$$

H is magnetic field intensity inside of MREs under the different temperatures, which can be obtained as follows

$$H = \frac{H_0}{\alpha_\mu\mu_{\text{eff}}} = \frac{H_0}{\alpha_\mu(1+\chi_{\text{eff}})} \tag{3}$$

α_μ is temperature coefficient of permeability. 20 °C (293 K) is considered as the initial temperature in this work. When an external magnetic field H_0 and a shear strain γ is imposed on the MREs, the magnetic susceptibility is changed. That leads to a magnetic field-induced shear stress τ, which can be expressed as

$$\tau = -\frac{1}{2}\mu_0{\alpha_\mu}^2\left(\frac{H_0}{1+\chi_{\text{eff}}}\right)^2\frac{\partial\chi_{\text{eff}}}{\partial\gamma} \tag{4}$$

Hence, the field-induced shear modulus ΔG can be expressed as

$$\Delta G = \tau/\gamma = -\frac{1}{2}\mu_0{\alpha_\mu}^2\left(\frac{H_0}{1+\chi_{\text{eff}}}\right)^2\frac{\partial\chi_{\text{eff}}}{\partial\gamma}/\gamma \tag{5}$$

χ_{eff} is the effective magnetic susceptibility in the direction of the applied field, which is defined as

$$\chi_{\text{eff}} = \frac{\overline{M}}{H_0} = \frac{J}{\mu_0 H_0} \tag{6}$$

$\overline{M}$ is the average magnetization intensity and J is the average particle polarization which is parallel to the direction of the applied field. So J can be expressed as

$$J = \frac{\sum_{l=1}^{2L}(p_l n_l)}{V} \tag{7}$$

where p_l and n_l, respectively, denote the total dipole moment in the z-axis direction and number of the columns that have l particles in the z-axis direction, and V is the volume of the whole MR elastomers.

Because the length of the columns obeys the Gaussian distribution, by using a constant factor k, n_l can be expressed as

$$n_l = k\frac{1}{\sqrt{2\pi}\sigma}\,\mathrm{e}^{-(l-L)^2/2\sigma^2} \tag{8}$$

The total number of particles in the z-axis direction in the whole MR elastomers can be obtained by the sum of that in all the

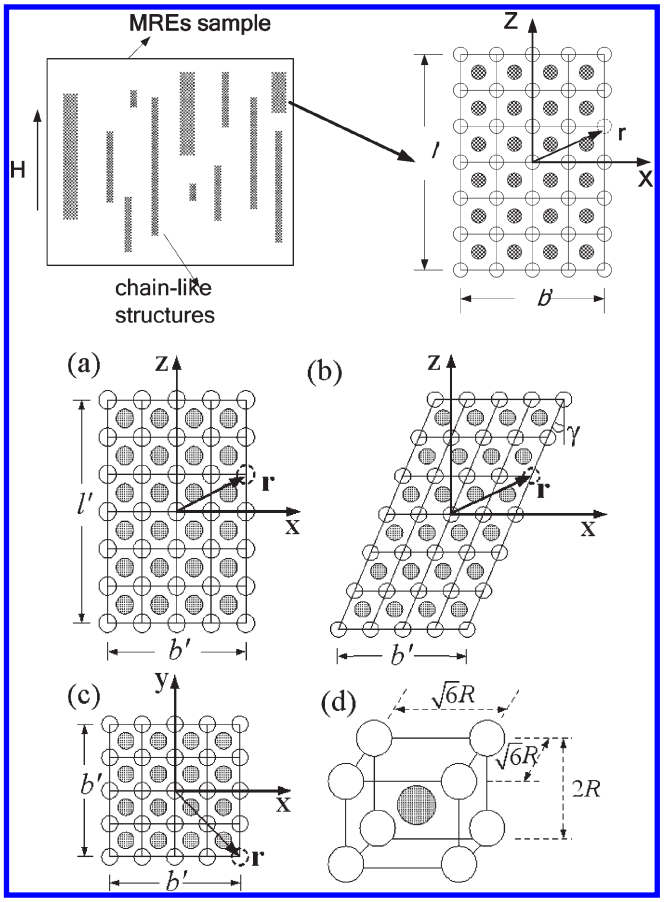

Figure 10. BCT column is viewed in the direction parallel to z-axis when the MREs samples are (a) without external displacement or (b) under a shear strain γ. (c) the cross-section perpendicular to z-axis, (d) the dimension of each BCT cell. The BCT lattice can be regarded as compound of chain of class A and B. The empty and shadowed circle is denoted as the particle in chain of class A and B, respectively. The particles have radius R and are not shown to scale.

columns

$$N = \sum_{l=1}^{2L} (ln_l) \tag{9}$$

It can be seen from Figure 10c that the number of particles in the cross section of a column is $b^2 + (b-1)^2$. So N can also be calculated by

$$N = \frac{V\varphi}{V_p(b^2 + (b-1)^2)} \tag{10}$$

where φ is the volume percentage of the particles, and V_p is the volume of each particle. From the eqs 8−10, k can be obtained and n_l is given by

$$n_l = \frac{\varphi V e^{-(l-L)^2/2\sigma^2}}{V_p(b^2 + (b-1)^2)\sum_{l=1}^{2L}(le^{-(l-L)^2/2\sigma^2})} \tag{11}$$

Under the external magnetic field, a dipole moment is induced on each sphere particle. And the dipole moment will produce an additional magnetic field on the other dipole moments. So the dipole moment is affected by both the external magnetic field and other dipole moments. As the particles compose the BCT structures periodically, and for the sake of simplicity, each particle in a column is assumed to have the same dipole moment.

p_l in eq 7 can be expressed by the sum of all the dipole moment in the columns, which have the number of l particles in the z-axis direction

$$p_l = \sum^{l} p_{i,z} = n_i^l p_{i,z} \tag{12}$$

where $p_{i,z}$ is the component in the z-axis direction of the dipole moment, and n_i^l, which is the number of particles in the columns that have number of l particles in the z-axis direction, is equal to $b^2 l + (b-1)^2(l-1)$. In the following, $p_{i,z}$ is calculated by using a dipole approximation with local-field effects.

$\mathbf{H}_{loc}$ is the local field which is the sum of the external field $\mathbf{H}_0$ and the field $\mathbf{H}_p$ from all other dipoles evaluated at the position of the center of particle under consideration

$$\mathbf{H}_{loc} = \mathbf{H}_0 + \mathbf{H}_p \tag{13}$$

where

$$\mathbf{H}_p = \sum \frac{1}{4\pi\mu_0 r^5}(-r^2\mathbf{p} + 3(\mathbf{p}\cdot\mathbf{r})\mathbf{r}) \tag{14}$$

$\mathbf{r}$ is the position vector relative to the origin and is summed over all other particle in the column under consideration. By setting the position of center particle in the column as the origin (as shown in Figure 10a−c), the component of eq 14 in z-axis is

$$H_{p,z} = \sum \frac{1}{4\pi\mu_0(x^2+y^2+z^2)^{5/2}}(-(x^2+y^2+z^2)p_z + 3z(p_x x + p_y y + p_z z)) \tag{15}$$

As the external field is in the direction of z-axis, the dipole moment's components in x-axis and y-axis are ignored. Then eq 15 are simplified as

$$H_{p,z} = \sum \frac{2z^2 - x^2 - y^2}{4\pi\mu_0(x^2+y^2+z^2)^{5/2}} p_z \tag{16}$$

$H_{p,z}$ is induced by the dipole moments in two class chains, A and B.

First, the effect of class A chains is discussed. The particle's coordinate (x,y,z) is determined by two parts which are the particle's relative position to the origin (A_1,A_2,A_3) and the shear strain γ. In Figure 10a, c, compared to the origin, the particle represented by broken circle is the second particle in the x-axis direction, the second one in the y-axis negative direction, and the first one in the z-axis direction. So its relative position to the origin can be expressed as (2,-2, 1) which is not changed by the shear strain. For class A chains, there is

$$\begin{aligned} x &= \sqrt{6}A_1 R + 2A_3 R \sin\gamma \\ y &= \sqrt{6}A_2 R \\ z &= 2A_3 R \cos\gamma \end{aligned} \tag{17}$$

Substituting eq 17 into eq 16, the range of the sum for integer A_1, A_2,A_3 is, respectively $[-(b-1)/2, (b-1)/2)]$, $[-(b-1)/2, (b-1)/2)]$, $[-(l-1)/2, (l-1)/2)]$ when b and l are odd numbers and$[-(b/2-1), (b/2-1)]$, $[-(b/2-1), (b/2-1)]$, $[-(l/2-1), (l/2-1)]$ when b and l are even numbers.

dx.doi.org/10.1021/ie200386x |*Ind. Eng. Chem. Res.* 2011, 50, 6704–6712

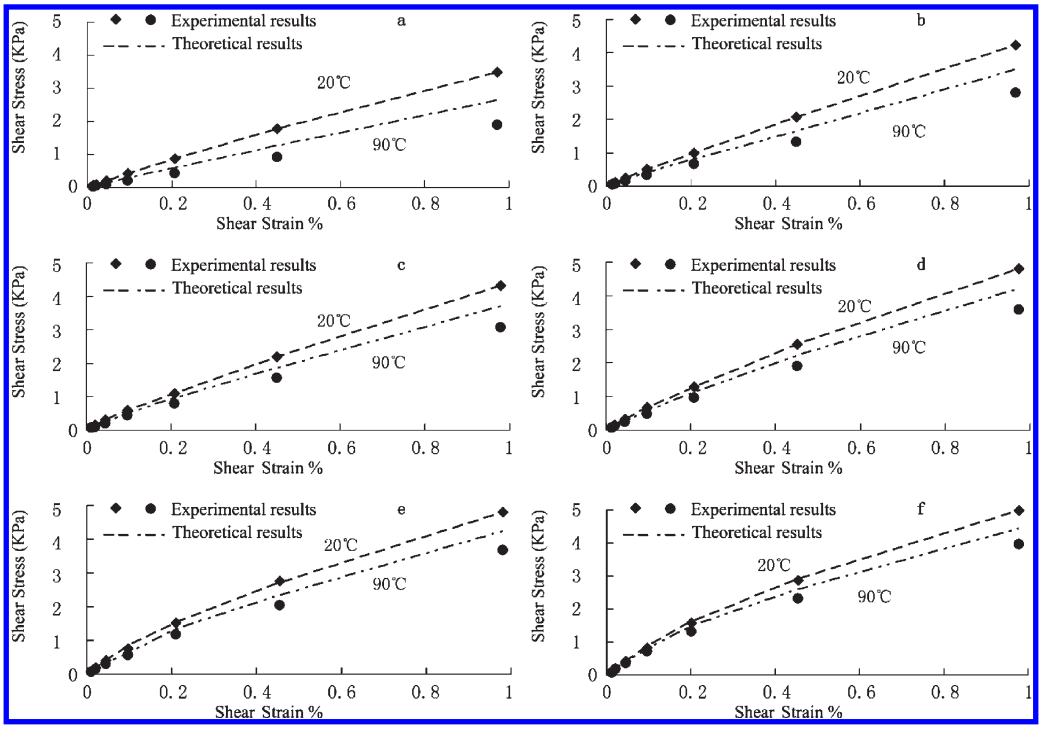

Figure 11. Relationship between stress and strain of samples at 800 mT BR:NR a (100:0), b (80:20), c (60:40), d (40:60), e (20:80), f (0:100).

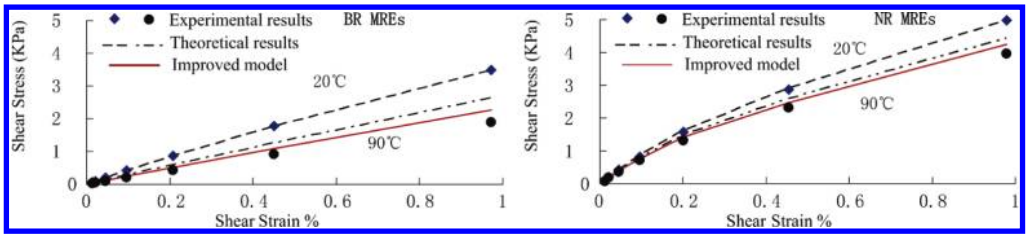

Figure 12. Relationship between stress and strain of samples at 800 mT.

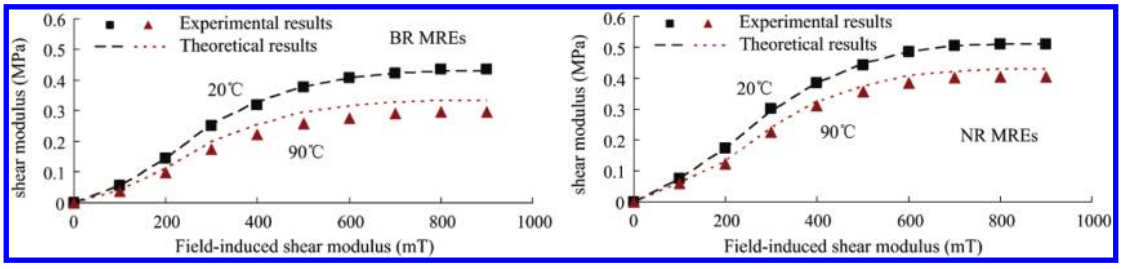

Figure 13. Relationship between shear modulus and magnetic fields at 20 and 90 °C.

Similarly, class B chains, there is

$$x = \frac{\sqrt{6}}{2}(2B_1 - 1)R + 2(B_3 - 1)R \sin\gamma$$
$$y = \frac{\sqrt{6}}{2}(2B_2 - 1)R$$
$$z = 2(B_3 - 1)R\cos\gamma \qquad (18)$$

Substituting eq 18 into eq 16, the range of the sum for integer B_1, B_2,B_3 is respectively $[-(b-1)/2, 0)$ &$(0, (b-1)/2)]$, $[-(b-1)/2, 0)$ &$(0, (b-1)/2)]$, $[-(l-1)/2, 0)$ &$(0, (l-1)/2)]$ when b and l are odd numbers and $[-b/2, 0)$ &$(0,b/2]$, $[-b/2, 0)$ &$(0, b/2]$, $[-l/2, 0)$ &$(0,l/2]$ when b and l are even numbers.

It is difficult to obtain the analytical expression for the relationship between $H_{p,z}$ and p_z from the eqs 16−18 directly. Instead, we first set given values to b and γ, and a series of values to l, i.e. letting l be from 1 to 200. Then a series of values of $\Sigma(2z^2 - x^2 - y^2)/(4\pi\mu_0(x^2 + y^2 + z^2)^{5/2})$ (denoted by $\Sigma g(x,y,z)$ later) can be computed. By using high-order (>10) polynomial fitting, the expression $f(l)$ as a function of l is yielded, which can accurately predict each value of $\Sigma g(x,y,z)$. If the columns have different values of width or shear strain, the sum is recalculated

dx.doi.org/10.1021/ie200386x |*Ind. Eng. Chem. Res.* 2011, 50, 6704–6712

and a new $f(l)$ can be yielded. Here, the relationship is briefly given by

$$H_{p,z} = f(l,b,\gamma)p_z \tag{19}$$

Under a low external magnetic field, a dipole moment induced linearly on each sphere particle is given by

$$p = 3\mu_e\mu_0\beta V_p H \tag{20}$$

where μ_p and μ_e denotes the relatively permeability of the particles and elastomers matrix respectively, and $\beta = (\mu_p - \mu_e)/(\mu_p + 2\,\mu_e) \approx 1$ when $\mu_p = 1 \times 10^3$ and $\mu_e = 1$. At a high magnetic field, the magnetic nonlinearity and saturation of the particle magnetization is described by the Frohlich−Kennely law[28]

$$M = \frac{p}{\mu_0 V_p} = \frac{\chi_l H}{1 + \chi_l H/M_s} \tag{21}$$

where χ_l is the magnetic susceptibility in the low external field and M_s is the saturation magnetization. When the field is low, $\chi_l H/M_s$ is inclined to zero, and then eq 21 can be degraded into

$$p = \mu_0 V_p \chi_l H \tag{22}$$

By comparing eq 20 and eq 22, χ_l is obtained. Substituting which to eq 21, the relation between the dipole moment and the magnetic field can be rewritten as

$$p = \frac{3\mu_e\mu_0\beta V_p H}{1 + 3\mu_e\beta H/M_s} \tag{23}$$

From eqs 13, 19, and 23, p_z is obtained as a function of external field (H_0), particle numbers in the column's length and width direction (l and b), and the imposed shear strain (γ). Combining this result with eqs 6, 7, 11, and 12, the effective magnetic susceptibility χ_{eff} is obtained. On the other hand

$$\frac{\partial\chi_{eff}}{\partial\gamma} = \frac{\partial\chi_{eff}}{\partial f(l,b,\gamma)}\frac{\partial f(l,b,\gamma)}{\partial\gamma} = \frac{\partial\chi_{eff}}{\partial f(l,b,\gamma)}\frac{\partial\sum g(x,y,z)}{\partial\gamma}$$
$$= \frac{\partial\chi_{eff}}{\partial f(l,b,\gamma)}\sum\frac{\partial g(x,y,z)}{\partial\gamma} = \frac{\partial\chi_{eff}}{\partial f(l,b,\gamma)}k(l,b,\gamma) \tag{24}$$

where $k(l,b,\gamma)$ is the polynomial fitting result of the $\Sigma(\partial g(x,y,z))/(\partial\gamma)$. By substituting the results of χ_{eff} and $(\partial\chi_{eff})/(\partial\gamma)$ into the eq 4, the field-induced shear stress is solved and the field-induced shear modulus (ΔG) is calculated accordingly. According to our previous result,[27] we assume that $\sigma^2 = 9$ and $L = 20$, $b = 3$ which are suitable for the properties of MREs. And the shear strain is set from 0 to 0.01. Here, we can get the calculate results of field-induced shear modulus ΔG and the relationship between Shear stress τ and shear strain γ (as shown in Figure 11).

$$\tau = G\gamma = (\Delta G + G_0)\gamma \tag{25}$$

G_0 is the initial modulus of MREs samples without applying a magnetic field.

It can be seen in Figure 11 that the theoretical results fit the experimental results very well at 20 °C, which has been considered as the initial temperature for the temperature coefficient of permeability α_μ. However, the theoretical results do not match the experimental results very well when the testing temperature is 90 °C. In the above model, we just consider the temperature effect on the magnetic interaction between the magnetic particles. The temperature effect on aging properties of MREs and the interaction between particles and matrix rubber under different temperatures have not been considered. Thus, the temperature influence on the interaction between particles and matrix rubber was further studied in this work.[22]

Arrhenius correction formula can be used to explain aging properties of MREs

$$k(T) = BT^{b/R}ge^{-(E_a' + bT)/RT} \tag{26}$$

$k(T)$ is the constant of reaction rate, T is the aging temperature, R is Moore constant of gas. B and E_a' are material constants.

The relationship between performance and aging time is

$$F_X(t) = k(T)gt \tag{27}$$

$F_X(t)$ is performance expression of samples, t is aging time.

Substituting eq 26 into 27

$$F_a(t_i) = BT^{b/R}ge^{-(E_a' + bT)/RT}gt_i \tag{28}$$

Therefore, this model can be improved by considering the temperature influence on the magnetorheological effect. Taking pure BR and NR MREs as examples, the relationships between Shear stress τ and shear strain γ are shown in Figure 12. It can be seen in Figure 12 that the modified model (the red curve) fit the experimental data better, and the simulation results are more accurate than before. The model is suitable for MREs based on different rubber matrix. Here, it also can be found that the shear stress of NR MREs sample is higher than that of BR MREs samples under the same shear strain and the decrease of stress caused by temperature rising is lower than that of BR samples, which demonstrated that NR samples has better mechanical properties and durability than that of BR samples under the same conditions.[22]

The relationship between shear modulus and magnetic fields at 20 and 90 °C, which were simulated by using the improved model is shown in Figure 13. It is found that simulation results fit the experimental data. When the testing temperature is 90 °C, the model also agrees the trend of experimental results well. The theoretical results is a little higher than experimental results, which is because that the model is built by assuming that the all particles inside of MREs samples obeys the Gaussian distribution and no defect in the matrix. In fact, not all the chain-like structures obey the Gaussian distribution exactly and some defect exists in the rubber matrix. Thus the theoretical result is a little higher. As a result, this model can predict the properties of MREs and only some simple material parameters are needed, which will enable it to be widely used in engineering applications.

4. CONCLUSION

In this work, mechanical properties of MREs based on different rubber matrix are evaluated, and an improved constitutive equation was developed to model properties in the different magnetic fields and different temperatures.

Storage modulus (G') and loss modulus (G'') of samples which contained only BR always decreased with temperature rises and the relationship between modulus and temperature, stress and strain were linear. But modulus of samples that contained NR first decreased with temperature rises and increased when testing temperature got higher. Modulus of other samples based on not only BR but also NR was between that of BR MREs and NR MREs.

An improved constitutive equation was developed to model properties in the different magnetic fields and different temperatures. This model only depends on some material parameters which can be easily measured in experiments. The comparison between experimental results and the model-prediction results demonstrated that the model can predict the trend of properties of MRE in the different conditions.

AUTHOR INFORMATION

Corresponding Author

*E-mail: gongxl@ustc.edu.cn (G.X.); xuansh@ustc.edu.cn (X.S.).

ACKNOWLEDGMENT

Financial support from SRFDP of China (20093402110010), NSFC (No.11072234), and the Fundamental Research Funds for the Central Universities are gratefully acknowledged.

REFERENCES

(1) Claracq, J.; Sarrazin, J.; Montfort, J. P. Viscoelastic properties of magnetorheological fluids. *Rheol. Acta* **2004**, *43*, 38.

(2) Li, W. H.; Chen, G.; Yeo, S. H. Viscoelastic properties of MR fluids. *Smart Mater. Struct.* **1999**, *8*, 460.

(3) Zhang, W.; Gong, X. L.; Xuan, S. H.; Xu, Y. G. High-performance hybrid magnetorheological materials: preparation and mechanical properties. *Ind. Eng. Chem. Res.* **2010**, *49*, 12471.

(4) An, H. N.; Picken, S. J.; Mendes, E. Enhanced hardening of soft self-assembled copolymer gels under homogeneous magnetic fields. *Soft Matter* **2010**, *6*, 4497.

(5) Gong, X. L.; Zhang, X. Z.; Zhang, P. Q. Fabrication and characterization of isotropic magnetorheological elastomers. *Polym. Test.* **2005**, *24*, 669.

(6) Wang, Y. L.; Hu, Y.; Gong, X. L.; Jiang, W. Q.; Zhang, P. Q.; Chen, Z. Y. Preparation and Properties of Magnetorheological Elastomers Based on Silicon Rubber/Polystyrene Blend Matrix. *J. Appl. Polym. Sci.* **2007**, *103*, 3143.

(7) Chen, L.; Gong, X. L.; Jiang, W. Q.; Yao, J. J.; Li, W. H. Investigation on magnetorheological elastomers based on natural rubber. *J. Mater. Sci.* **2007**, *42*, 5483.

(8) Li, J. F.; Gong, X. L.; Xu, Z.; Jiang, W. Q. The effect of prestructure process on magnetorheological elastomer performance. *Int. J. Mater. Res.* **2008**, *12*, 1358.

(9) Kramarenko, E.Yu.; Stepanov, G. V.; Abramchuk, S. S.; Grishin, D. A.; Nikitin, L. V.; Khokhlov, A .R. Effect of a homogeneous magnetic field on the viscoelastic behavior of magnetic elastomers. *Polym. Test.* **2007**, *48*, 488.

(10) Deng, H. X.; Gong, X. L.; Wang, L. H. Development of an adaptive tuned vibration absorber with magnetorheological elastomer. *Smart Mater. Struct.* **2006**, *15*, 111.

(11) Ginder, J. M.; Nichols, M. E.; Elie, L. D.; Tardiff, J. L. Magnetorheological elastomers: Properties and applications. In *Smart Structures and Materials 1999: Smart Materials Technologies*; Wuttig, M. R., Ed.; SPIE: Bellingham, WA, 1999; Vol. 3675, p 131

(12) Watson, J. R. U.S. Patent 5 609 353, 1997.

(13) Carlson, J. D.; Jolly, M. R. MR fluid, foam and elastomer devices. *Mechatronics* **2000**, *10*, 555.

(14) Zhang, X. Z.; Li, W. H. Adaptive tuned dynamic vibration absorbers working with MR elastomers. *Smart Struct. Syst.* **2009**, *5*, 517.

(15) Li, W. H.; Wang, X. Y.; Zhang, X. Z.; Zhou, Y. Development and analysis of a variable stiffness damper using an MR bladder. *Smart Mater. Struct.* **2009**, *18*, 074007.

(16) Zschunke, F.; Rivas, R.; Brunn, P. O. Temperature behavior of magnetorheological fluids. *Appl. Rheol.* **2005**, *15*, 116.

(17) Davis, L. C. Model of magnetorheological elastomers. *J. Appl. Phys.* **1999**, *85*, 3348.

(18) Dorfmann, A.; Brigadnov, I. A. Constitutive modelling of magneto-sensitive Cauchy-elastic solids. *Comput. Mater. Sci.* **2004**, *29*, 270.

(19) Li, W. H.; Zhang, X. Z. A study of the magnetorheological effect of bimodal particle based magnetorheological elastomers. *Smart Mater. Struct.* **2010**, *19*, 035002.

(20) Li, W. H.; Zhou, Y.; Tian, T. F. Viscoelastic properties of MR elastomers under harmonic loading. *Rheol. Acta* **2010**, *49*, 733.

(21) Sahin, H.; Wang, X. J.; Gordaninejad, F. Temperature Dependence of Magneto-rheological Materials. *J. Intell. Mater. Syst. Struct.* **2009**, *20*, 2215.

(22) Zhang, W.; Gong, X;L.; Jiang, W. Q.; Fan, Y. C. An investigation of the durability of anisotropic magnetorheological elastomers based on mixed rubber. *Smart Mater. Struct.* **2010**, *19*, 085008.

(23) Chen, L.; Gong, X. L.; Li, W. H. Damping of magnetorheological elastomers. *Chin. J. Chem. Phys.* **2008**, *21*, 581.

(24) Motoc, D. L. Dynamic Mechanical Analysis of Multiphase Polymeric Composite Materials. *Mater. Plast.* **2009**, *46*, 462.

(25) Morton, M. *Rubber Technology*; Van Nostrand Reinhold: New York, 1973; p 127.

(26) Li, J. F.; Gong, X. L. Dynamic damping property of magnetorheological elastomer. *J. Cent. South Univ. Technol.* **2008**, *15*, 261.

(27) Zhang, W.; Gong, X. L.; Chen, L. A Gaussian distribution model of anisotropic magnetorheological elastomers. *J. Magn. Magn. Mater.* **2010**, *322*, 3797.

(28) Tao, R.; Sun, J. M. 3-dimensional structure of induced electrorheological solid. *Phys. Rev. Lett.* **1991**, *67*, 398.

(29) Zhou, L.; Wen, W.; Sheng, P. Ground states of magnetorheological fluids. *Phys. Rev. Lett.* **1998**, *81*, 1509.

(30) Guan, X. C.; Dong, X. F.; Ou, J. P. Magnetostrictive effect of magnetorheological elastomer. *J. Magn. Magn. Mater.* **2008**, *320*, 158.

(31) Bossis, G.; Lemaire, E.; Volkova, O. Yield stress in magnetorheological and electrorheological fluids: A comparison between microscopic and macroscopic structural models. *J. Rheol.* **1997**, *41*, 687.